Aswan University Journal of Sciences and Technology Volume 5, issue 3, September 2025

Investigating the Lateral Behavior of Offshore Monopiles Subjected to Cyclic Lateral Loads in Sandy Soil: An Experimental Study

Manar Naser[1*], Ashraf Ahmed[1], Kamal Hafez[2]

[1] Civil Engineering Department, Faculty of Engineering, Aswan University, Egypt.

[2] Ismailia Faculty of Engineering, Suez Canal University, Egypt.

Abstract

Due to the increasing demand of renewable energy, offshore wind turbines (OWTs) of large dimensions are widely used nowadays. These types of structures are subjected to very high environmental lateral loads caused by wind, wave and current loads, and bending moments. To support these loads, deep foundations of large dimensions are necessary. Large diameter monopiles are currently the most popular foundation type used to support OWTs. Owing to the increasing necessity of large dimension monopiles, their behavior should be paid much attention, and their dimensions should be carefully optimized. Thus, an extensive parametric study considering both monotonic and cyclic lateral loads should be perseveringly performed. The main aim of this paper is to present a sensitivity analysis that provides an insight on the effect of different parameters affecting the monopile behavior under monotonic/cyclic lateral loads throughout the utilization of a 1g experimental model. The effect of monopile diameter and embedded length on the monopile behavior is studied and analyzed. According to the experimental results, the effect of monopile embedded length has a higher reduction impact on the lateral monopile behavior in both monotonic and cyclic lateral loading cases than of the monopile diameter. Thus, designers should pay attention to the embedded length more than the monopile diameter.

Keywords: Monopile; Monotonic load; Cyclic lateral load; 1g experimental model; Sand.

1. Introduction

Offshore wind energy technologies have become more common in recent years due to the increasing need for sustainable energy sources to reduce gas and carbon emissions [1-3]. The construction of large offshore wind turbines with large blades is the result of advancements in industrial technology. Supporting these enormous turbines is a difficult task since they are subjected to numerous environmental loading types. Suction buckets, jackets, tripods, and monopiles are examples of the foundation types used to support these huge structures. Because of the low cost, simplicity of installation, high stability, and straightforward manufacturing process, monopiles are the most popular one of these foundation types [4, 5].

The harsh conditions of the offshore environments make OWT foundations expose to a wide variety of loads, which have crucial effects on their performance. These loads include (i) bending moments, (ii) lateral loads from wind, waves, and currents and (iii) vertical loads due to the own weight of the wind turbine. Because of the cyclic nature of waves, wind, and currents, the lateral loads acting on the offshore monopile foundations are cyclic.

*Corresponding author E-mail: manar.mohamed@eng.aswu.edu.eg

Received February 20, 2025, received in revised form, May 08, 2025, accepted May 08, 2025.

(ASWJST 2021/ printed ISSN: 2735-3087 and on-line ISSN: 2735-3095) https://journals.aswu.edu.eg/stjournal

These cyclic lateral loads result in an accumulation of lateral response of the offshore monopiles. The resulting lateral deformation must remain within the allowable bounds defined by design standards to meet serviceability requirements. Thus, monopiles must be designed with large dimensions in order to withstand such circumstances and to extend the service life of the OWTs. The effect of these large dimensions and the cyclic load characteristics on the monopile performance must be extensively studied.

Several investigations have been conducted to predict the response of large diameter monopiles to cyclic lateral loading. Among others, LeBlanc et al. [6] used a monopile with diameter of 80mm and embedded length of 360mm in their experimental tests. The experiments were carried out in sand with relative densities of 4% and 38%, representing in-situ loose and medium-dense sand, respectively. Preparing soil samples at lower relative densities is recommended to ensure that the friction angle in the experimental tests corresponds to the in-situ relative denisty. It was confirmed that the dispacement of a rigid monopile is largely influenced by the characteristics of the applied cyclic lateral load.

Moreover, Albiker et al. [7] focused on the influence of the cyclic lateral load on the rate of the accumulated lateral displacement. A monopile with diameter D=60 mm and embedded length L=350mm was tested in medium-dense sand. The tests had demonstrated that for rigid monopile-soil systems, the maximum accumulation rate appears for partially symmetric two-way cyclic lateral load. Additionally, Klinkvort and Hededal [8] used two solid steel piles with diameters of 28 mm and 40 mm in dense-sand subjected to cyclic lateral loadings to provide a simple design procedure for predecting the accumulation of the lateral displacement.

Nigitha, et al. [9] conducted finite element simulations to assess the lateral response of monopiles under one and two-way cyclic loading, highlighting the influence of pile embedment. Similarly, Alsharedah, et al. [10] developed a detailed 3D finite element model to investigate the effect of pile geometry and soil strength on laterally loaded monopiles. On the experimental front, Wang, et al. [11] integrated results from reduced-scale field tests and centrifuge experiments to evaluate the lateral behavior of monopiles in sandy soils. Despite the previous studies found in literature, more rigorous study is still to be extended. The present study fills this gap by presenting an extensive sensitivity analysis to explore the effect of monopile dimensions (i.e., monopile embedded length L and monopile diameter D) on the lateral behavior of the monopile embedded in sandy soil.

The following sections present the small-scale model tests and a presentation and analysis of the experimental results for the different loading cases studied in this paper.

2. Small-scale model tests

This section presents a detailed description of the 1g experimental model used herein to study the lateral monopile behavior. Moreover, the soil properties and test program showing the tested monopile dimensions are presented.

2.1. Experimental equipment

A practical and productive mechanical loading system has been utilized for applying loads to monopiles. Rovere [12] developed a mechanical rig consisting of an 80 cm wide, 100 cm length

and 100 cm height container filled with sand, a steel frame with pulleys, three weight hangers, and a lever with a driving motor, as displayed in **Figure 1**. The lever is connected to the frame by a pivot and carries a motor that swings a weight m_1 to offer cyclic loading. The motor employed is a geared, single-phase AC motor. It swings with a frequency of 0.106 Hz [6, 12-15]. The ropes are low-stretch ropes of 0.3 cm diameter.

The rig is static equipment with simple design. First, the masses m_1 and m_2 are set to zero, and the mass m_3 is adjusted to equalize any force utilized on the lever. In this situation, the lever deflections are small (i.e. $\Theta \approx \frac{\pi}{2}$) measured from the vertical direction. To apply a sinusoidal force [F(t)] to the monopile, the masses m_1 and m_2 are calculated as presented in **Equations (1)** and **(2)** below:

$$m_1 = \frac{(l_2/l_a)F_a}{g} \qquad \textbf{(1)}$$

$$m_2 = \frac{(l_c/l_a)F_a - F_0}{g} \qquad \textbf{(2)}$$

Where F_0, F_a are the loading rig forces, l_2, l_a, l_c are the loading rig dimensions, and g denotes the gravitational acceleration. The applied force at any time (t) can be calculated from **Equation (3)** below:

$$F(t) = F_0 + F_a \sin(\omega t) \qquad \textbf{(3)}$$

Where ω is the rotational frequency. As m_2 can not to be negative, both l_a and l_c have to achieve the criteria of $l_a/l_c < F_a/F_0$ [6]. The monopile lateral displacement is measured using two displacement sensors located at 1cm and 13cm above the soil surface. A load cell is tied between the lever and the monopile to measure the load applied to the monopile head.

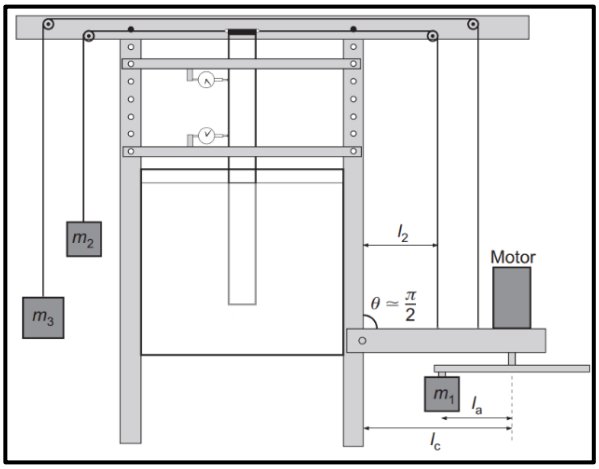

Figure 1: A schematic diagram of the cyclic loading rig [6].

2.2. Soil properties and preparation

This section is devoted to describing the soil properties and preparation process. Notice that the experimental study was conducted on dry sand to represent the drained condition of the sand [6, 16, 17]. Though there may be some variations in the performance of free-draining saturated cohesionless materials when drained compared to air-dried conditions, both reflect an identical tendency to accumulate strain when exposed to cyclic loading [18]. The sand properties adopted in this study are listed in **Table 1**. The particle size distribution profile of the sand specimen is presented in **Figure 2**.

To prepare consistent sand samples, dry sand was poured layer by layer into a steel test box using mass control. Each layer, 5cm deep, had been compacted in a repeatable way with a smoothing wheel [19]. The soil weight of each layer before compaction was calculated according to the required soil relative density D_r. In the present study, 40% relative density was used, resulting in a soil effective unit weight $\gamma`$=16.7 kN/m^3. The unit weight and relative density were kept constant throughout the testing process.

Table 1: Soil properties.

Property	Unit	Value
Mean particle size (D_{50})	mm	0.54
Uniformity coefficient (C_u)	-	1.57
Coefficient of curvature (C_c)	-	1.16
Specific Gravity (G_s)	-	2.63

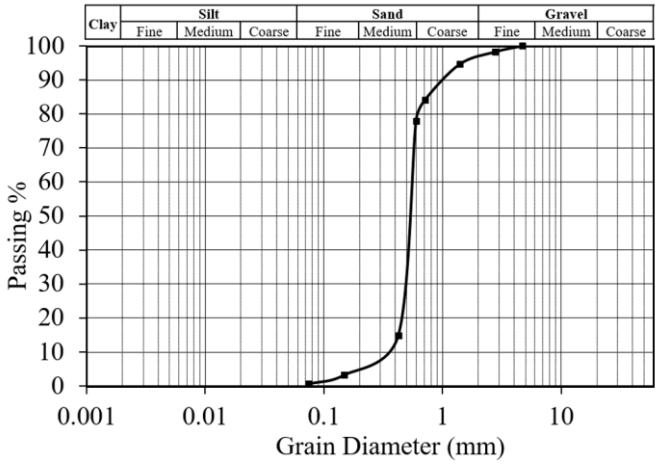

Figure 2: Soil particle size distribution chart.

To reduce the potential effects of the monopile installation, the sand box was filled with sand to about 5cm above the anticipated location of the monopile toe. The open-ended monopile was then carefully inserted 5cm into the soil and firmly fastened in place before finishing the soil preparation around the pre-installed monopile [7, 17].

2.3. Test program

The program of the experimental tests carried out in this paper is presented in this section. It is essential to define some factors that characterize the cyclic load and cyclic response of the monopile-soil system. The cyclic load is characterized by cyclic load magnitude (ξ_b) and cyclic load ratio (ξ_c) defined in **Equations** (4**)** and (5**)**, respectively.

$$\xi_b = \frac{H_{max}}{H_{ult}} \quad \textbf{(4)}$$

$$\xi_c = \frac{H_{min}}{H_{max}} \quad \textbf{(5)}$$

In which H_{ult} represents the ultimate monotonic lateral load of the monopile. Note that H_{ult} is defined as the lateral load corresponding to a lateral displacement of 0.1D in the monotonic load test [20]. On the other hand, H_{max} and H_{min} indicate the maximum and minimum values of the cyclic load, respectively.

Figure 3 presents a schematic diagram showing the characteristics of the monopile cyclic response (where the monopile response shown in this figure is the lateral displacement). In this figure, y_1 and y_N represent the monopile lateral displacements at the end of the loading stage of the first cycle (cycle_1) and the cycle number N (cycle_N), respectively. However, y_{R1} and y_{RN} denote the residual monopile lateral displacements at the end of the unloading stage of the first cycle and the cycle number N, respectively. Moreover, Δy_N refers to the accumulated lateral displacement after N loading cycles. It is equal to the difference between y_N and y_1. Finally, δy_N represents the incremental lateral displacement between any two successive cycles. It can be calculated as the difference between y_N and y_{N-1}.

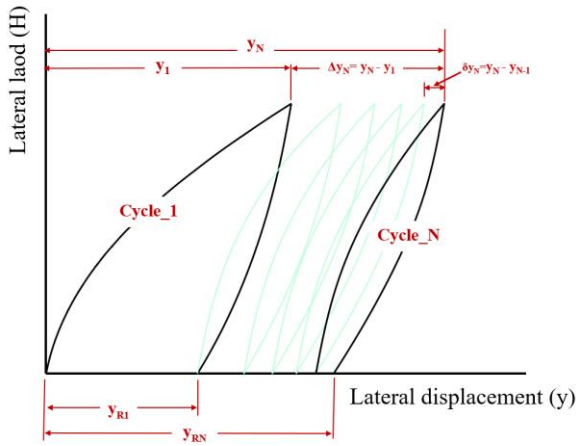

Figure 3: Schematic diagram showing the characteristics of the lateral displacement.

Extensive experimental tests, including monotonic and cyclic lateral loads, were performed. Each test examined a monopile embedded in dry sand with a relative density of about 40%. The monopile models are fabricated of steel tubes C450. **Figure 4** presents the schematic diagram of the monopile.

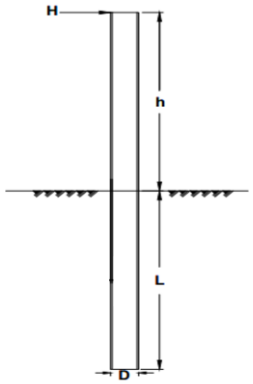

Figure 4: Schematic diagram of the monopile.

Three monopile models with different dimensions were used in the experimental tests as presented in **Table 2**. These models include a Reference Case (RC) with dimensions of D=4cm and L=24cm. The purpose of this study is to investigate the effect of the monopile dimensions (i.e., D and L) on the lateral behavior of the monopile. To study the lateral behavior of the monopile, it is essential to select an appropriate value of H_{max} as will be discussed later in this paper. **Table 2** presents the experimented test program adopted in this paper. Notice that each test was performed under "fresh" sittings (i.e., no preloading), and each test was repeated at least two times in order to prove redundancy.

Table 2: Monopile dimensions and program of the experimental tests.

Test No.	Type	D (mm)	L (mm)	h (mm)	H_{max} (N)	H_{min} (N)	ξ_c	N	Notes
M1	Monotonic	40	240	240	0	0	0	-	RC
M2	Monotonic	40	360	240	0	0	0	-	
M3	Monotonic	60	240	240	0	0	0	-	
C1	Cyclic	40	240	240	36.1	0	0	2000	R_C, ξ_b=0.95
C2	Cyclic	40	360	240	36.1	0	0	2000	
C3	Cyclic	60	240	240	36.1	0	0	2000	

3. Experimental results

This section focuses on presenting the experimental results. The effect of the monopile geometry on the lateral monopile behavior in case of monotonic lateral load is first presented and analyzed. Then, the influence of L and D on the lateral monopile behavior in case of cyclic lateral load is presented and discussed.

3.1. Monotonic loading case

The aim of this section is to present the ultimate monotonic lateral capacity of the reference case monopile and to study its sensitivity to the change of L and D. Notice that, in order to examine the impact of a certain parameter, all other parameters were kept constant and equal to those of the reference case.

3.1.1. Lateral capacity of the reference case monopile

As mentioned previously in section 2.3, a monopile with dimensions D=4 cm, L=24 cm and h=24 cm was chosen as a Reference Case (RC). The lateral displacement (y) is measured at the soil surface. **Figure 5** shows the backbone curve (i.e. the load-displacement curve under monotonic lateral loading). From this figure, it is not possible to define a distinct failure point to define the ultimate lateral load. Thus, the ultimate lateral load is defined as the lateral load which induces a lateral displacement of 0.1D (i.e. 4 mm) **[20].** This load is equal to 38N as can be deduced from **Figure 5**.

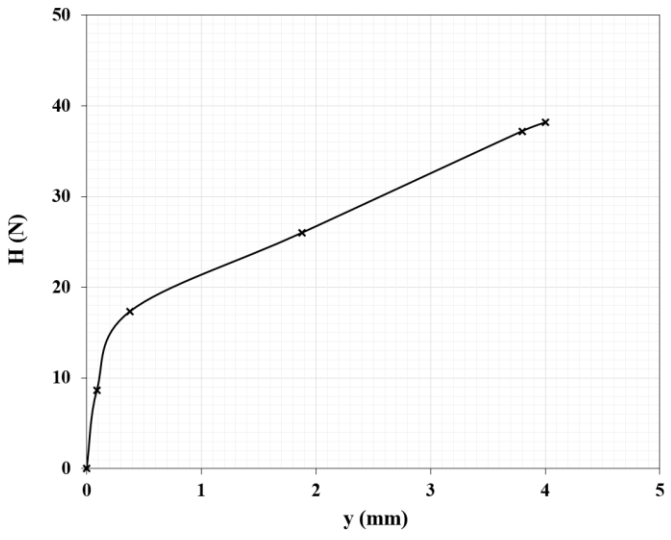

Figure 5: The backbone curve of the RC at mudline.

3.1.2. Effect of Monopile Embedded Length

In this subsection, the effect of the monopile embedded length on its lateral behavior under monotonic lateral loading is investigated. The embedded length has been increased by 50% of its original value (i.e. from 24cm to 36cm as defined in test M2 presented in **Table 2**). **Figure 6** shows the effect of the monopile embedded length on the backbone curve at mudline. According to this figure, increasing the embedded length by 50% (i.e. from 24 cm to 36 cm) increases the monopile ultimate lateral capacity by 52.6% (i.e. from 38 N to 58 N).

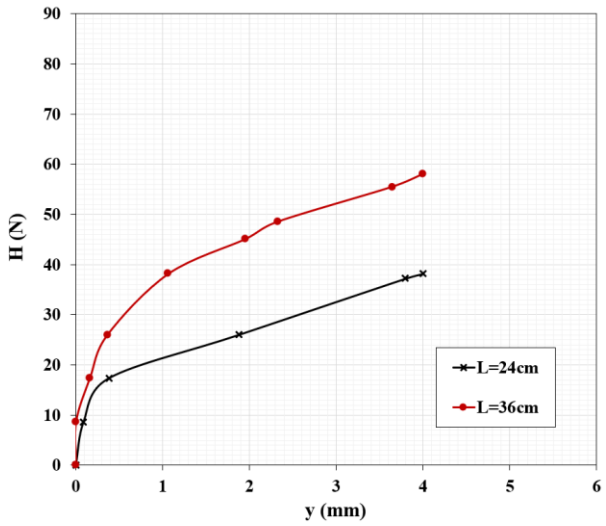

Figure 6: Effect of the monopile embedded length on the backbone curve at mudline.

3.1.3. Effect of Monopile Diameter

In this subsection, the effect of monopile diameter on its lateral behavior under monotonic lateral loading is examined. The monopile diameter has been increased by 50% of its reference value (i.e from 4cm to 6cm as defined in test M3 presented in **Table 2**). **Figure 7** shows the effect of monopile diameter on the backbone curve at mudline. From this figure, increasing the monopile diameter by 50% results in a 36.8% increase in the ultimate lateral capacity of the monopile (i.e. from 38 N to 52 N).

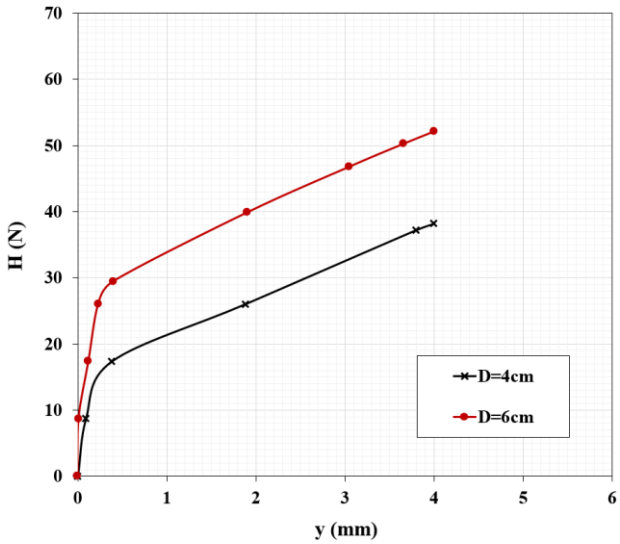

Figure 7: Effect of the monopile diameter on the backbone curve at mudline.

3.2. Cyclic loading case

The sensitivity of the monopile response to the change in the monopile dimensions under cyclic lateral load is investigated in this section. To accurately study the effect of monopile dimensions, it is more convenient to apply the same load in all tests. According to the test results from the monotonic load presented in section 3.1, the lateral capacity of the considered monopiles ranges from 38N to 58N. If too high value of the maximum cyclic lateral load (H_{max}) is applied, the monopile will fail and show no elastic behavior. However, if it is too small, a small accumulated displacements will be obtained which make the results difficult to be compared. In this paper, H_{max} was kept constant and taken equal to 36.1N for all studied cases.

The variation of the monopile lateral displacement (y) and rotation (Θ) with the number of cycles (N) is plotted in **Figure 8** and **Figure 9**, respectively. This figure indicates that log(N) is linearly proportional to log(y) and to log(Θ). This ensures the hypothesis proposed by [6] that in the absence of experimental data, it might be reasonable to extrapolate data to a high number of cycles (e.g. $N=10^7$).

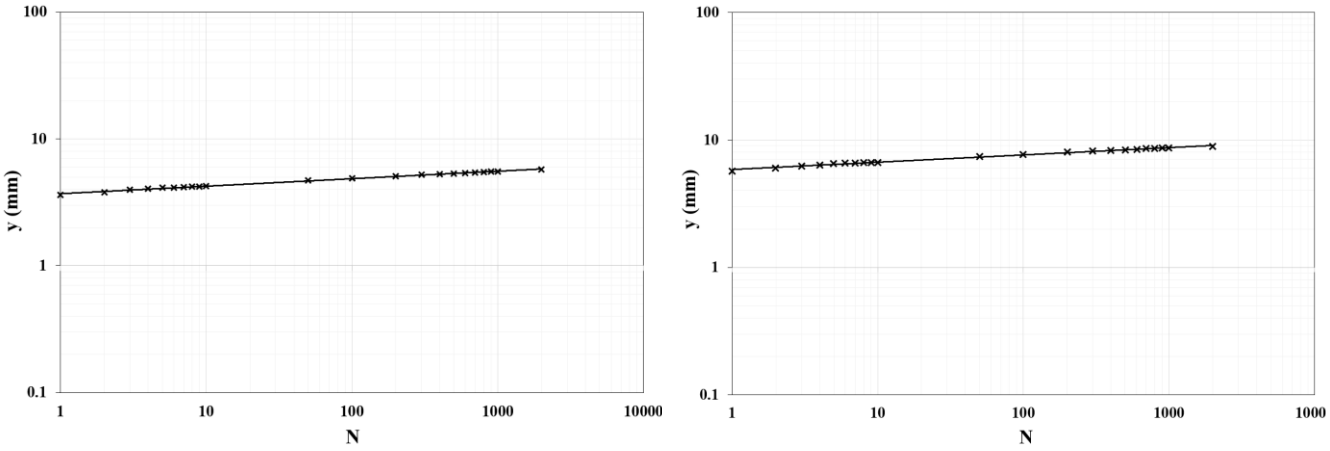

Figure 8: Variation of the monopile lateral displacement with number of cycles for RC at **(a)** ground surface and **(b)** 13cm above the ground surface

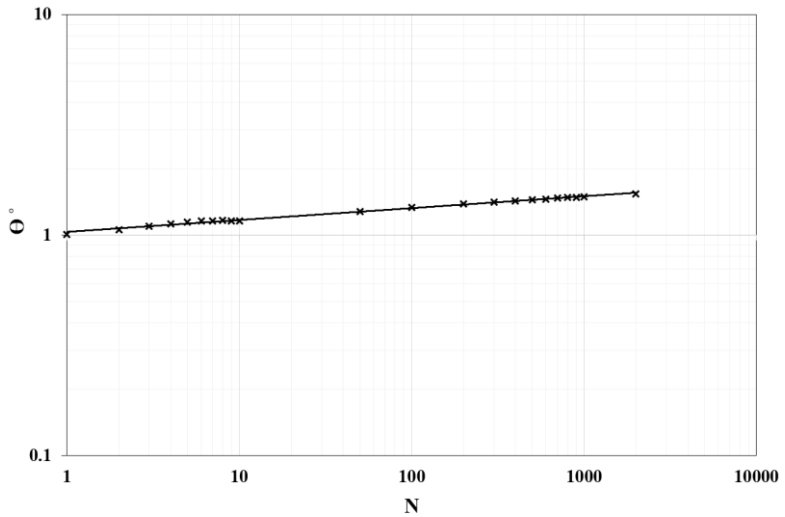

Figure 9: Variation of the monopile rotation with number of cycles for RC.

The increase in the lateral monopile deformation is caused by the change in the density of soil, rotation of principal stress directions in soil and changing of stress condition on pile-soil interface after [21]. **Figure 10** and **Figure 11** provide respectively the variation of the normalized accumulated lateral monopile displacement ($\tilde{y}$=Δy/$y_{N=1}$) and rotation ($\tilde{\theta}$=Δϴ/$\Theta_{N=1}$) with number of cycles. The accumulated normalized lateral monopile displacement and rotation are calculated according to **Equations (6)** and **(7)** as proposed by [17] and **[6],** respectively. From **Figure 10** and **Figure 11**, a high increase in the normalized accumulated displacement and rotation can be observed for the first 10 cycles. For the number of cycles larger than 10, the rate of increase is smaller.

$$\tilde{y} = \frac{\Delta y}{y_{N=1}} = \frac{y_N - y_{N=1}}{y_{N=1}} \quad (6)$$

$$\tilde{\theta} = \frac{\Delta\theta}{\theta_{N=1}} = \frac{\theta_N - \theta_{N=1}}{\theta_{N=1}} \quad (7)$$

In which $\tilde{y}$ refers to normalized lateral monopile displacement. Δy is the accumulated lateral displacement. $y_{N=1}$ and y_N are the lateral displacement at first and N cycles, respectively. Moreover, $\tilde{\theta}$ indicates the normalized monopile rotation. Δθ is the accumulated pile rotation. $\theta_{N=1}$ and θ_N are the monopile rotation at first and N cycles, respectively.

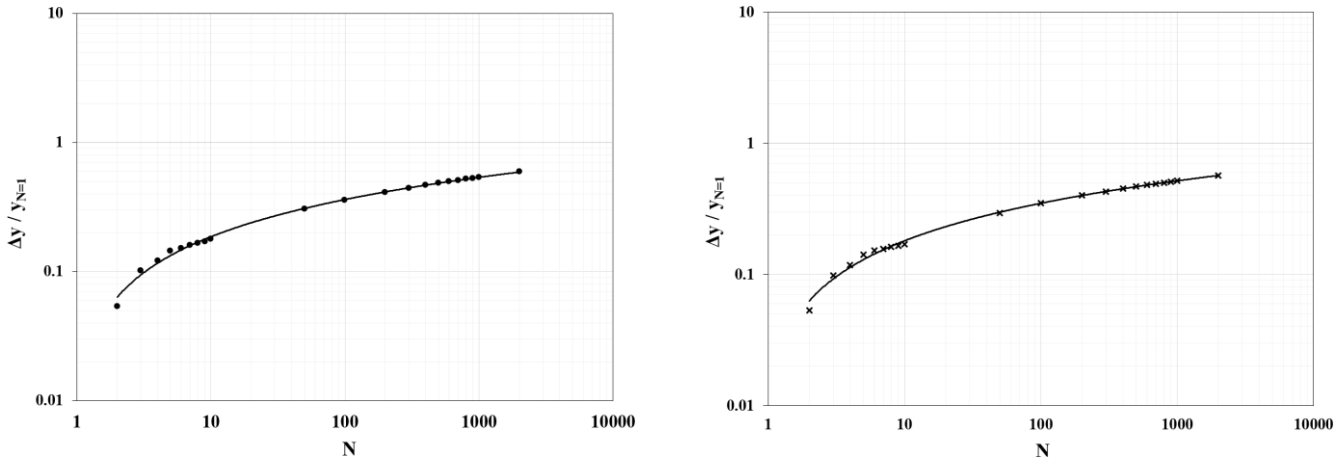

Figure 10: Variation of $\tilde{y}$ with the number of cycles for RC at **(a)** ground surface and **(b)** 13 cm above the ground surface.

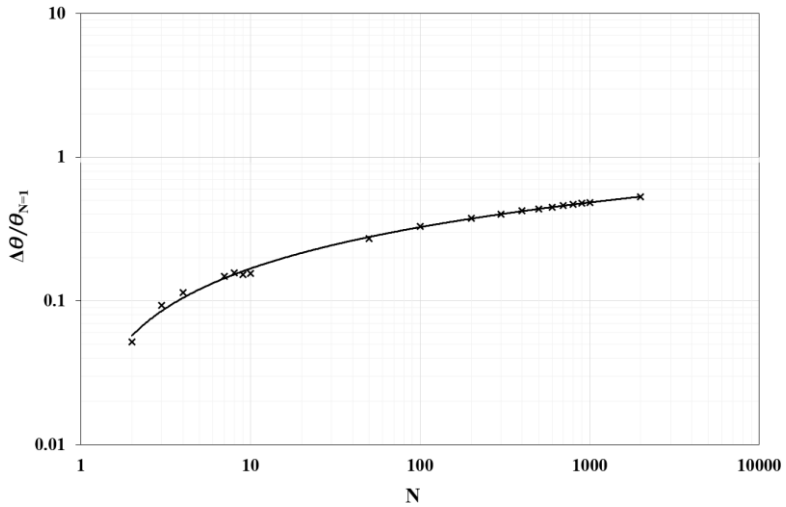

Figure 11: Variation of $\tilde{\theta}$ with the number of cycles for RC.

Figure 12 shows the variation of the lateral displacement (y) and the residual displacement (y_R) with the number of cycles. It is logical that plastic (permanent) displacement occurs when unloading the monopile. This is caused by the remaining residual stresses after the completion of the previous cycle [22]. Moreover, this plastic displacement increases with the increase of number of cycles.

The previously observed phenomenon may be explained by the nature of cohesionless soil, which is granular material that allows it to deform under cyclic loading. When a monopile is subjected to a cyclic loading, the soil in front of the monopile is rearranged and compacted. This leads to a decrease in the soil volume and an increase in its density. Since large voids initially exist around the monopile, there will be considerable rearrangement and compaction of soil during the initial cycles of loading causing the monopile to move rapidly. With each load cycle, the soil in front of the pile becomes denser (more compacted) leading to more deformation resistance. As a result, the deformation rate of the monopile gradually decreases, indicating that the pile has almost reached a state of relative stability even if it may continue to deform slowly. This is because there is still some volume of voids in the soil that can be compressed and reduced under cyclic loading. Furthermore, under a high number of cycles the soil particles may be crushed and the monopile deforms at a low rate. This ensures that the behavior of monopile under cyclic loading in cohesionless soil follows sedation behavior. The sedation behavior is observed in several laboratory tests (e.g. [23] among others).

Figure 13 shows the distribution of the lateral displacement along the monopile embedded length. This figure confirms the aforementioned observations. At the soil surface, the lateral displacement increased by 53.68% from 1 to 1000 cycles, and by only 3.47% from 1000 to 2000 cycles which means that the lateral deformation accumulates at a decreasing rate. Moreover, it is obvious from this figure that the pivot point (i.e. zero-deflection point) gradually moves downward by increasing the number of cycles. This observation is in conformity with that of [24].

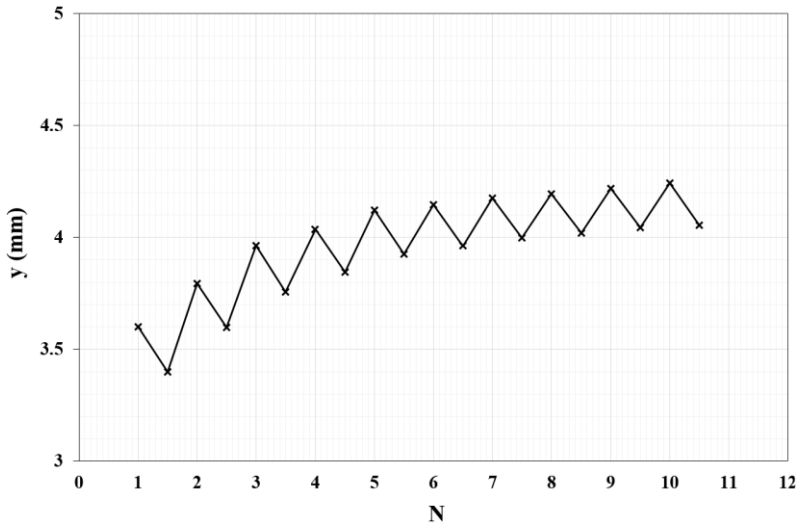

Figure 12: Variation of lateral displacement for loading and unloading stages with number of cycles at mudline for RC.

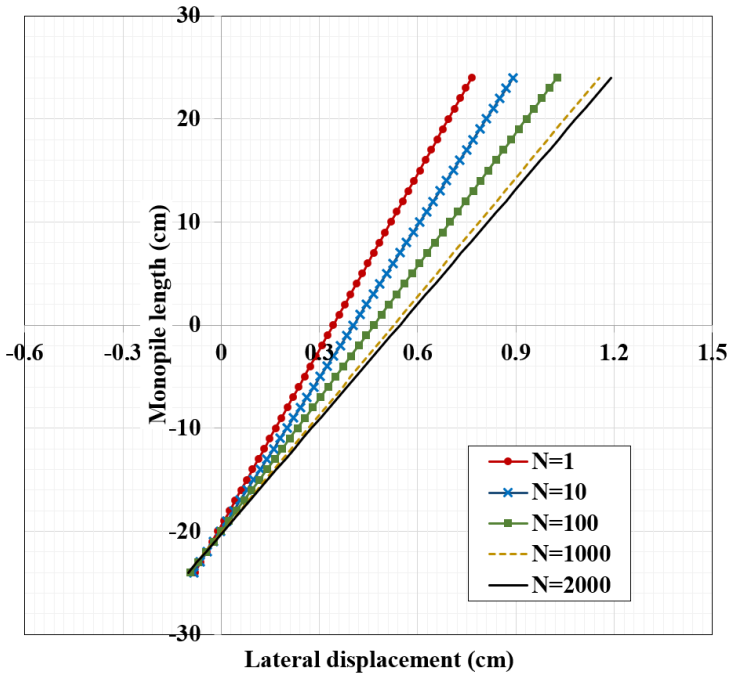

Figure 13: Distribution of the lateral displacement along the monopile embedded length for RC.

3.2.1. Effect of Monopile Embedded Length

To investigate the effect of monopile embedded length on the monopile lateral behavior, the lateral deformation for the RC monopile is compared to that of a monopile with L=36 cm (detailed in test C2 presented in **Table 2**). **Figure 14** and **Figure 15** present respectively a comparison between the variation of the lateral displacement and rotation of the two monopiles. These figures indicate that increasing the monopile embedded length decreases its lateral displacement and rotation and thus, leads to improve its behavior. For instance, when N=1000 cycles, increasing L by 50%, decreases the lateral displacement at mudline by 71.71%. This may be explained by the fact that the increase of the monopile embedded length results in a larger interaction area with the surrounding soil. This provides an additional lateral support to the monopile which reduces the lateral displacement of the monopile.

Figure 16 shows the variation of y and y_R with the number of cycles. The difference between y and y_R is higher in case of L=24 cm than that in the case of L=36 cm. For larger monopile length, the displacement is small, and the soil state is closest to the elasticity zone than the plasticity zone. On the contrary, for smaller monopile length, the displacement is high, and the soil state is almost fully plastic. In the plastic soil state, the soil damping, which refers to the ability of the soil to dissipate energy during loading and unloading, is higher than the elastic soil state. Higher damping indicates that the soil can absorb more energy during loading and release it during unloading. In the case of L=24cm, the soil has higher damping properties since the soil is almost in the plastic zone. Thus, it can absorb more energy during loading, leading to a higher displacement compared to the case of L=36cm. However, during unloading, the soil in case of L=24 cm can release more energy, resulting in a smaller unloading displacement compared to the case of L=36 cm. This difference in energy absorption and release can lead to a higher difference between loading and unloading displacements for L=24 cm compared to L=36 cm.

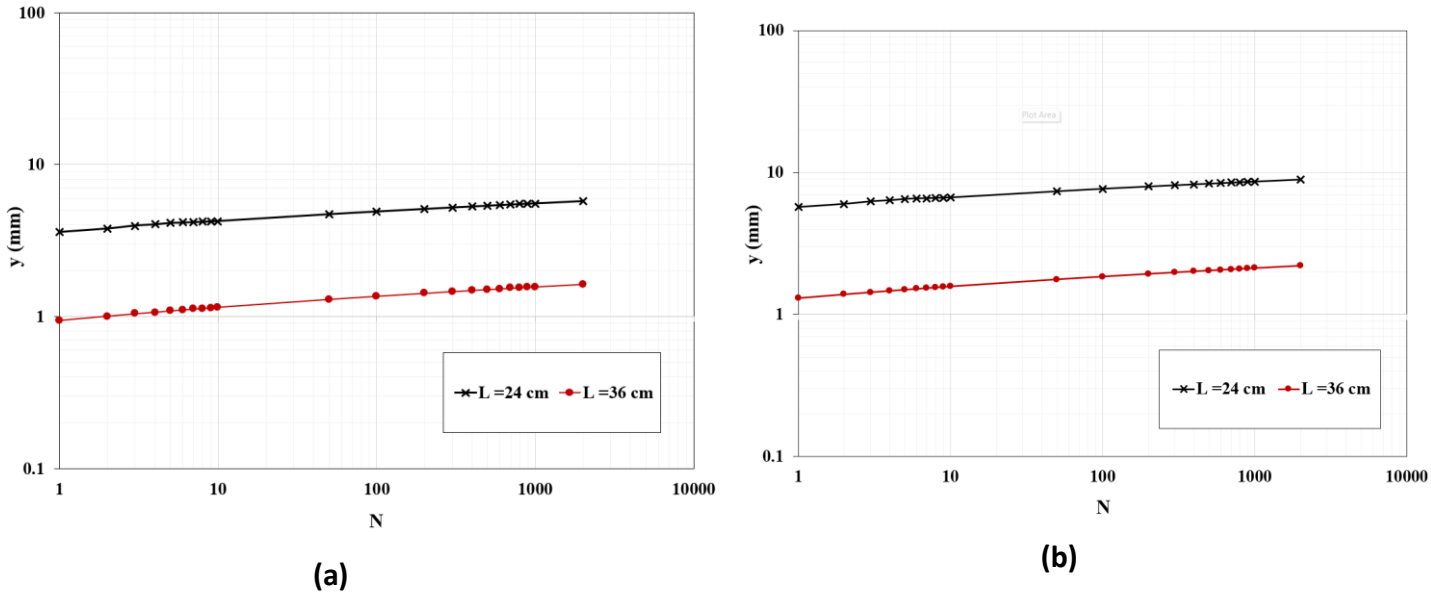

Figure 14: Comparison of lateral displacement response between two monopile embedded lengths (L =24 cm and L =36 cm) under cyclic loading at **(a)** ground surface and **(b)** 13cm above the ground surface.

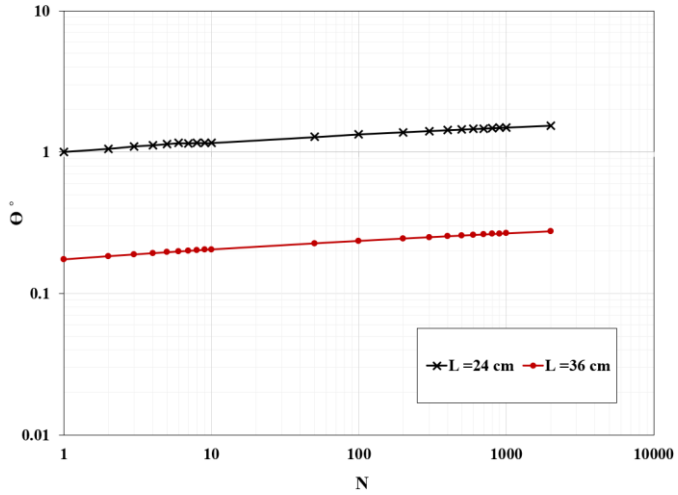

Figure 15: Effect of the monopile embedded length on the variation of the monopile rotation.

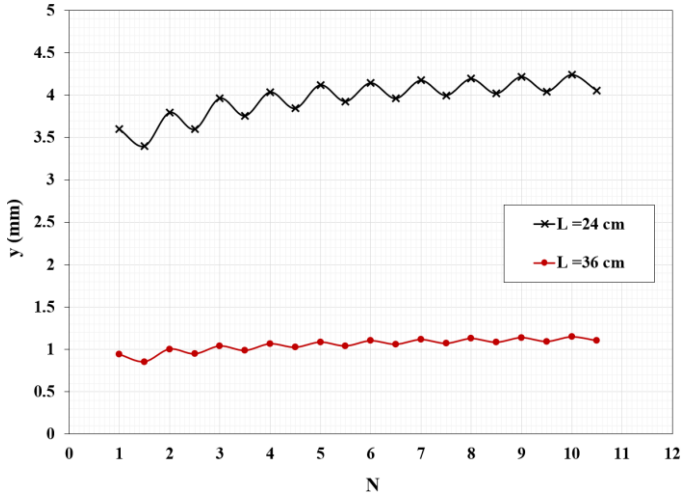

Figure 16: Effect of the monopile embedded length on the variation of the loading and unloading lateral displacement.

Figure 17(a-e) demonstrates the distribution of the lateral displacement along the monopile embedded length for L=24 cm and 36 cm at the various cycles number. The pivot point for L=24 cm is closer to the sand surface than L=36 cm. In the case of L=24 cm, the monopile exhibits more rotation than that of L=36 cm under the same lateral load. For L=24 cm, the pivot point is about 20cm from the soil surface for N=1000. On the other hand, at the same number of cycles the pivot point is observed at about 33 cm from the soil surface for L=36 cm. This agrees well with the analysis of [25].

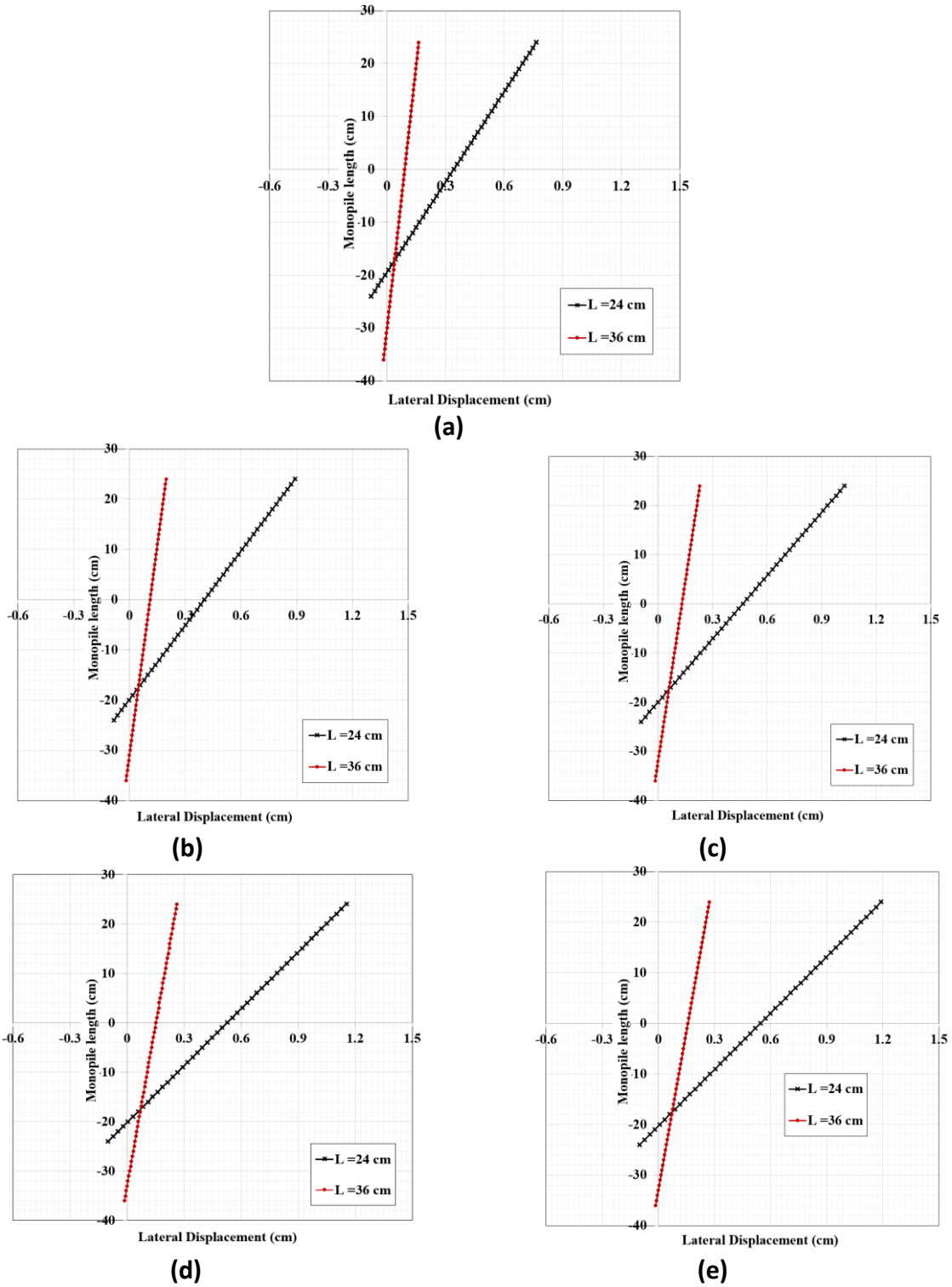

Figure 17: Distribution of the lateral displacement along the monopile embedded length for L=24cm and L=36cm at **(a)** N=1, **(b)** N=10, **(c)** N=100, **(d)** N=1000 and **(e)** N=2000.

3.2.2. Effect of Monopile Diameter

A monopile with D=60 mm subjected to a cyclic lateral load (defined in test No. 10 presented in **Table 2**) was used to investigate the effect of monopile diameter on its lateral behavior. **Figure 18** and **Figure 19** present respectively a comparison between the variation of lateral displacement and rotation for the RC and a monopile with D=60 mm. These figures show that the increase of the monopile diameter enhances its behavior by decreasing its displacement and rotation. From these figures, at N=1000, increasing the diameter by 50% results in a reduction of the lateral displacement at mudline and 13cm above the soil surface by 60% and 60.78%, respectively. The increase of the monopile diameter makes the monopile transmit the load more effectively to a larger area of the soil and thus the soil is subjected to smaller stresses, resulting in less displacement. Additionally, the increased diameter of the pile can increase the overall stiffness of the pile-soil system, which can also reduce displacement under cyclic loads.

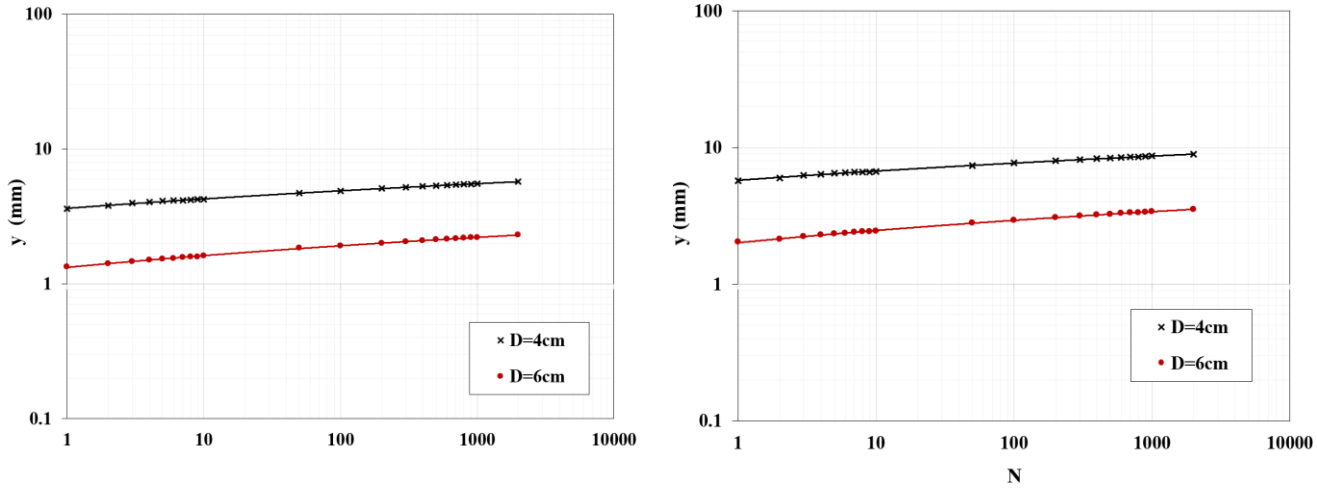

Figure 18: Comparison of lateral displacement response between two monopile diameters (D= 4 cm and D= 6 cm) under cyclic loading at **(a)** ground surface and **(b)** 13 cm above the ground surface

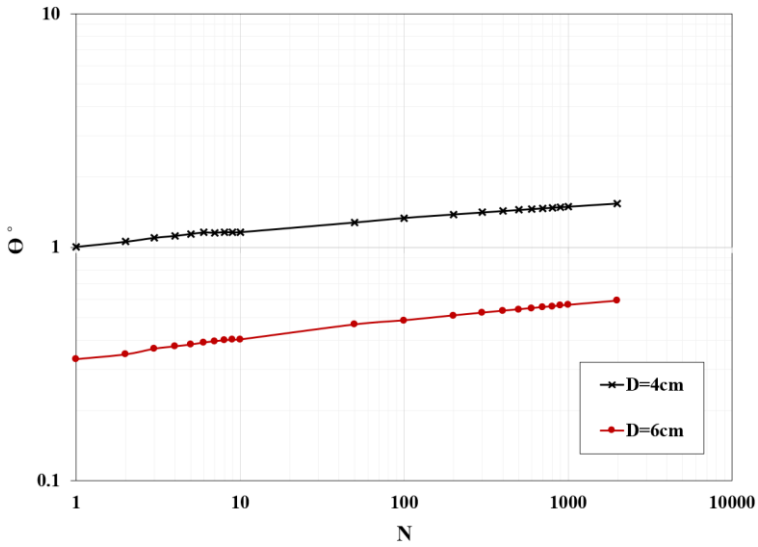

Figure 19: Effect of the monopile diameter on the variation of the monopile rotation.

Figure 20 shows the effect of the monopile diameter on the variation of the loading-unloading lateral displacement with the number of cycles for the RC and a monopile with D=60 mm. The difference between the displacement at the end of the loading stage and the residual displacement (i.e. the displacement at the end of the unloading stage) is higher in the case of D=40 mm than D=60 mm. The reason is similar to that explained previously for **Figure 16**.

Figure 21 (a-e) demonstrates the lateral displacement along the monopile embedded length for D=40 mm and D=60 mm at the different cycles number (i.e. at N=1, N=10, N=100, N=1000 and N=2000 cycles). The pivot point for D=40 mm is closer to the sand surface than D=60 mm. For D=40 mm, the pivot point is at about 0.83L from the soil surface for N=1000. On the other hand, at the same number of cycles the pivot point is observed at about 0.87L from the soil surface for D=60 mm. This agrees well with the analysis of [25].

4. Conclusions

This study provides an experimental analysis of large diameter monopiles embedded in dry sand and subjected to monotonic/cyclic lateral load. The effect of monopile dimensions (i.e., monopile embedded length and diameter) on the lateral behavior of the monopile is investigated in this study. The experimental results have shown that:

1. The lateral deformation of the monopile accumulates at a decreasing rate (for example, the lateral displacement increased by 53.68% from 1 to 1000 cycles, and by only 3.47% from 1000 to 2000 cycles).
2. The effect of monopile embedded length has a higher reduction impact on the lateral monopile behavior in both monotonic and cyclic lateral loading cases than of the monopile diameter (for instance, increasing embedded length and diameter by 50% decrease the lateral displacement at mudline by 71.71% and 60% respectively at N=1000).

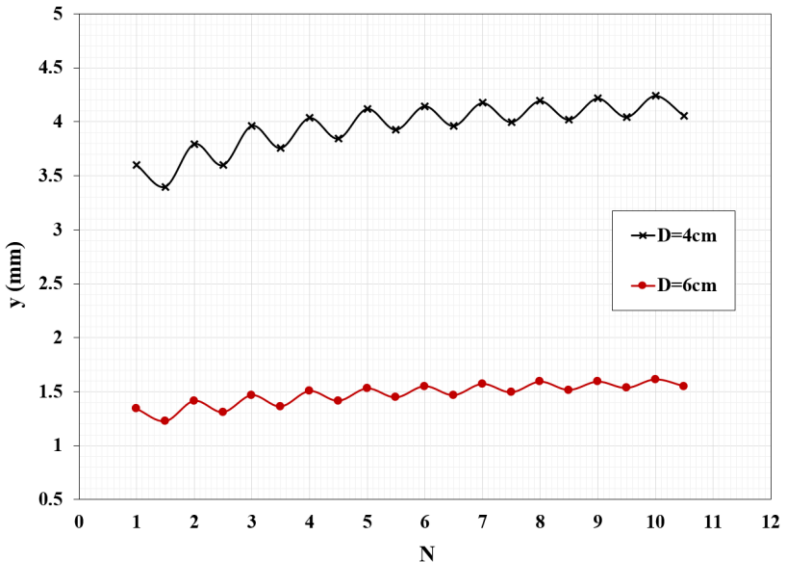

Figure 20: Effect of the monopile diameter on the variation of the loading and unloading lateral displacement.

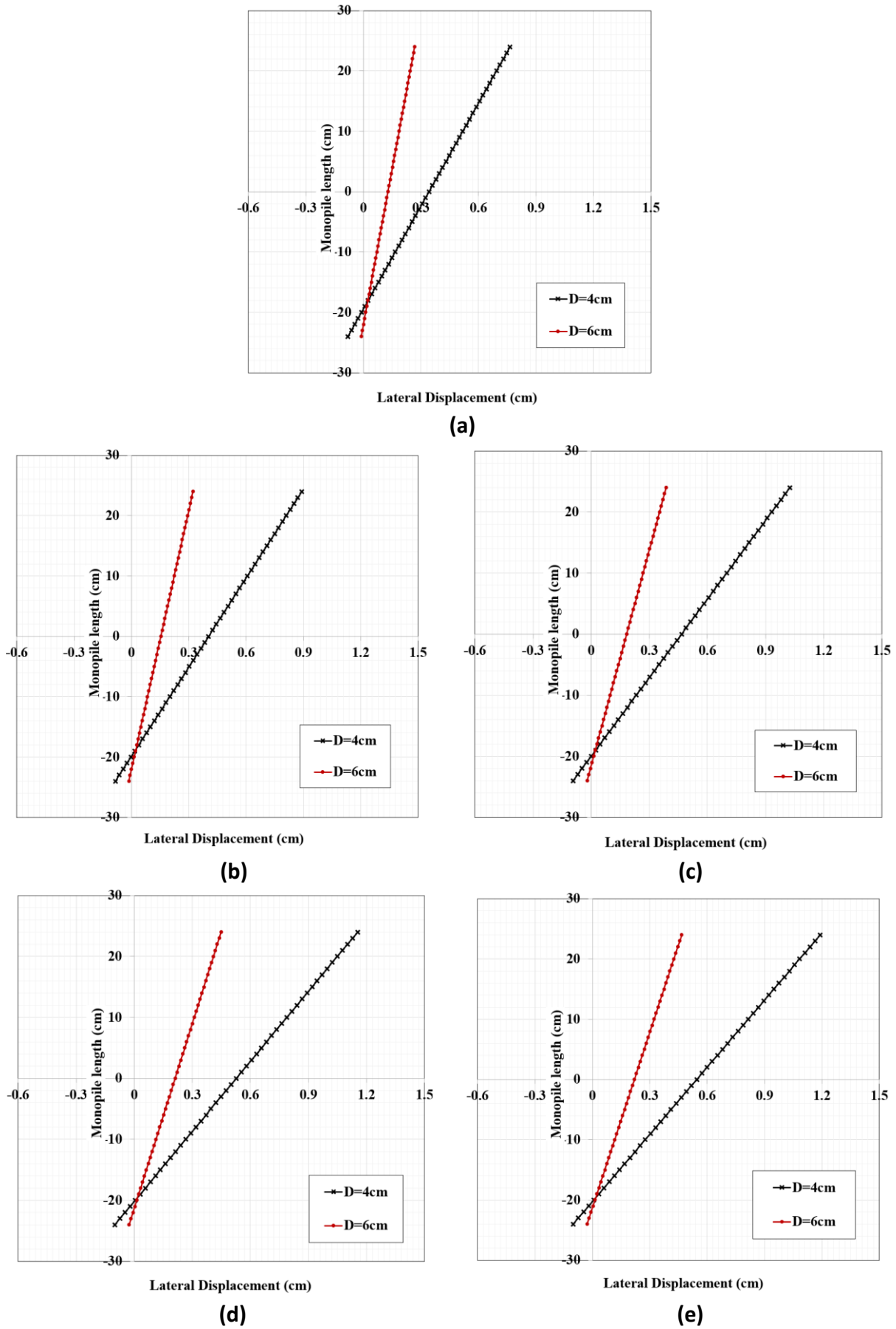

Figure 21: Distribution of the lateral displacement along the monopile embedded length for D=4cm and D=6cm at **(a)** N=1, **(b)** N=10, **(c)** N=100, **(d)** N=1000 and **(e)** N=2000.

References

1. Esteban, M.D.; Diez, J.J.; Jose, S.L.; Vicente, N. Why offshore wind energy? *Renew. Energy* 2011, *36*, 444–450.
2. Dinh, V.N.; McKeogh, E. Offshore wind energy: Technology opportunities and challenges. In *Proceedings of the 1st Vietnam Symposium on Advances in Offshore Engineering: Energy and Geotechnics*, Hanoi, Vietnam, 2019; pp. 3–22.
3. Yousefi, H.; Abbaspour, A.; Seraj, H. Worldwide development of wind energy and CO_2 emission reduction. *Environ. Energy Econ. Res.* 2019, *3*, 1–9.
4. Bakmar, C.L. *Design of Offshore Wind Turbine Support Structures: Selected Topics in the Field of Geotechnical Engineering*; 2009.
5. Esteban, M.D.; López-Gutiérrez, J.-S.; Negro, V. Gravity-based foundations in the offshore wind sector. *J. Mar. Sci. Eng.* 2019, *7*, 64.
6. LeBlanc, C.; Houlsby, G.; Byrne, B. Response of stiff piles in sand to long-term cyclic lateral loading. *Géotechnique* 2010, *60*, 79–90.
7. Albiker, J.; Achmus, M.; Frick, D.; Flindt, F. 1g Model Tests on the Displacement Accumulation of Large-Diameter Piles Under Cyclic Lateral Loading. *Geotech. Test. J.* 2017, *40*, 20160102.
8. Klinkvort, R.T.; Hededal, O. Lateral response of monopile supporting an offshore wind turbine. *Proc. Inst. Civ. Eng. Geotech. Eng.* 2013, *166*, 147–158.
9. Nigitha, D.; Rathod, D.; Krishnanunni, K.T. Finite-element analysis of a monopile under one-and two-way lateral cyclic loading. *Proc. Inst. Civ. Eng. Marit. Eng.* 2023, *176*, 138–157.
10. Alsharedah, Y.; Newson, T.; El Naggar, M. A 3-D modelling of monopile behaviour under laterally applied loading. *Geomech. Geophys. Geo-Energy Geo-Resour.* 2024, *10*, 1–20.
11. Wang, H.; Lehane, B.; Bransby, M.; Wang, L.; Hong, Y.; Askarinejad, A. Lateral behavior of monopiles in sand under monotonic loading: Insights and a new simple design model. *Ocean Eng.* 2023, *277*, 114334.
12. Rovere, M. *Cyclic Loading Test Machine for Caisson Suction Foundations*; Ecole Centrale de Lille/Politecnico di Milano: 2004.
13. Abongo, K.O. *Model Study of the Static and Cyclic Lateral Capacity of Finned Piles*; Lehigh University: 2019.
14. Lada, A.; Ibsen, L.B.; Nicolai, G. The stiffness change and the increase in the ultimate capacity for a stiff pile resulting from a cyclic loading. 2014.
15. Leblanc, C.; Byrne, B.; Houlsby, G. Response of stiff piles to random two-way lateral loading. *Géotechnique* 2010, *60*, 715–721.
16. Wang, Y.; Zhu, M.-X.; Gong, W.-M.; Dai, G.-L.; Wu, J.-B.; Zhu, W.-B. Cyclic lateral responses of monopiles considering the influence of pile–soil relative stiffness in sand. *Chin. Ocean Eng.* 2022, *36*, 247–257.
17. Frick, D.; Achmus, M. An experimental study on the parameters affecting the cyclic lateral response of monopiles for offshore wind turbines in sand. *Soils Found.* 2020, *60*, 1570–1587.
18. Kuo, Y.-S. *On the Behavior of Large-Diameter Piles under Cyclic Lateral Load*; Hannover University, Germany, 2008.
19. Chenrong, Z.; Xun, Z.; Maosong, H.; Huawei, T. Responses of caisson-piles foundations to long-term cyclic lateral load and scouring. *Soil Dyn. Earthq. Eng.* 2019, *119*, 62–74.
20. Zdravkovic, L.; et al. Numerical modelling of large diameter piles under lateral loading for offshore wind applications. 2015.
21. Kuo, Y.-S. *On the Behavior of Large-Diameter Piles under Cyclic Lateral Load*; Hannover University, Germany, 2008.
22. Collins, I.; Boulbibane, M. Shakedown under moving loads with applications to pavement design and wear. In *Developments in Theoretical Geomechanics*; 2000; pp. 1–20.

23. Hettler, A. Gründungskörper mit zyklischer Belastung in Sand und 1g-Modelltechnik. *Bautechnik* 2000, *77*, 901–908.
24. Achmus, M.; Kuo, Y.-S.; Abdel-Rahman, K. Behavior of monopile foundations under cyclic lateral load. *Comput. Geotech.* 2009, *36*, 725–735.
25. Ahmed, A.; Ismail, K.; Naser, M. Numerical analysis of offshore monopiles constructed in sand with stress-dependent stiffness. In *Proceedings of the AICSGE 2019—Tenth Alexandria International Conference on Structural and Geotechnical Engineering and Management*, Alexandria, Egypt, December 2019.